Controllable synthesis of ultrathin vanadium oxide nanobelts via an EDTA-mediated hydrothermal process*

Yu-Xiang Qin(秦玉香)†, Cheng Liu(刘成), Wei-Wei Xie(谢威威), and Meng-Yang Cui(崔梦阳)

School of Electronics and Information Engineering, Tianjin University, Tianjin 300072, *China*

(Received 8 August 2015; revised manuscript received 1 October 2015; published online 20 December 2015)

Ultrathin VO_2 nanobelts with rough alignment features are prepared on the induction layer-coated substrates by an ethylenediaminetetraacetic acid (EDTA)-mediated hydrothermal process. EDTA acts as a chelating reagent and capping agent to facilitate the one-dimensional (1D) preferential growth of ultrathin VO_2 nanobelts with high crystallinities and good uniformities. The annealed induction layer and concentration of EDTA are found to play crucial roles in the formation of aligned and ultrathin nanobelts. Variation in EDTA concentration can change the VO_2 morphology of ultrathin nanobelts into that of thick nanoplates. Mild annealing of ultrathin VO_2 nanobelts at 350 °C in air results in the formation of V_2O_5 nanobelts with a nearly unchanged ultrathin structure. The nucleation and growth mechanism involved in the formations of nanobelts and nanoplates are proposed. The ethanol gas sensing properties of the V_2O_5 nanobelt networks-based sensor are investigated in a temperature range from 100 °C to 300 °C over ethanol concentrations ranging from 3 ppm to 500 ppm. The results indicate that the V_2O_5 nanobelt network sensor exhibits high sensitivity, good reversibility, and fast response-recovery characteristics with an optimal working temperature of 250 °C.

Keywords: semiconductors, nanobelt, crystal growth, gas sensor

PACS: 73.61.Cw, 91.67.Jk, 68.35.B–, 61.72.up **DOI:** 10.1088/1674-1056/25/2/027307

1. Introduction

Assembling low-dimensional nanomaterials have attracted increasing interest due to their large specific surface areas and dimensions comparable to the Debye length,[1,2] and have various applications in nanodevices.[3,4] Vanadium oxide nanobelts with a rectangular cross section have attracted wide attention because of their versatile redox-dependent properties and potential applications in lithium batteries,[5] catalysts,[6] gas sensors,[7] and thermochromic devices.[8] As is well known, the size especially the thickness, crystallinity and alignment of nanobelts have great effects on their properties. Thus, the exploration of effective strategies on tailoring the microstructure such as the thickness and geometric arrangement of vanadium oxide nanobelts is desirable.

Chemical routes, such as the surfactant-assisted hydrothermal process are usually used to synthesize low-dimensional nanostructures. Up to now, different vanadium oxide nanostructures, such as V_2O_5 nanorods, V_2O_5 nanowires, and VO_2 nanobelts, have been reported to be synthesized via the hydrothermal method.[9–11] For the solution-based synthesis, organic modifiers like urea, sodium dodecylsulfate, and chelating agents have been proved to be effective in controlling the final shape of the nano- and microcrystals, such as nanobelts,[12] sheaf-like nanostructures,[13] and nanorods.[14] They serve as "capping reagent" to break the limitation of the intrinsic growth habit and then govern the crystal growth dynamically. However, the hydrothermally synthesized low-dimensional vanadium oxide nanostructures usually show a morphology of disordering assembly.[12,15–17]

In the present work, with the further consideration of the necessity of ordering arrangement for one-dimensional (1D) nanobelts, we develop a two-step process, i.e., inductive nucleation followed by EDTA-mediated hydrothermal growth, to realize aligned assembly of ultrathin VO_2 nanobelts on a substrate. The induction layer performed on the substrate provides initial nucleation sites, and the EDTA serves as chelating and capping agent to modify the growth dynamics of vanadium oxide along different directions. The *in-situ* formation mechanism of VO_2 nanobelts involving the effect of EDTA concentration is proposed. Furthermore, ultrathin V_2O_5 nanobelts are prepared via a mild annealing of ultrathin VO_2 nanobelts at 350 °C in air. To the best of our knowledge, a similar research on EDTA-mediated growth of aligned ultrathin VO_x nanobelts has not been reported. The as-synthesized nanobelts with ultrathin structures and certain alignments will have significant applications in nanodevices. Especially, V_2O_5 is known as a promising gas-sensing material for gas sensor application due to its attractive sensing performances to various gases. Thus, to demonstrate the potential applications of the as-prepared ultrathin vanadium oxide nanobelts, the gas-sensing properties of V_2O_5 nanobelt networks to ethanol are further evaluated and analyzed.

*Project supported by the National Natural Science Foundation of China (Grant Nos. 61274074, 61271070, and 61574100).

†Corresponding author. E-mail: qinyuxiang@tju.edu.cn; qyxtj@126.com

© 2016 Chinese Physical Society and IOP Publishing Ltd

2. Experiment

To prepare VO_2 nanobelts, a two-step process was performed. In the first step, an induction layer was prepared on a cleaned alumina substrate by spin-coating 0.05-M NH_4VO_3 solution with a pH value of 2.1–2.5 followed by thermal annealing at 600 °C in air for 2 h. The spin coating was repeated four times to ensure a uniform distribution and adequate coverage of the induction particles on the substrate after annealing. Prior to spin-coating of the NH_4VO_3 solution, a pair of interdigitated Pt electrodes each with a thickness of 100 nm was deposited on the cleaned alumina using the magnetic sputtering method. In the following step, the induction particles-coated substrate was submerged in a mixture solution of NH_4VO_3 and EDTA, which was sealed in a 100-ml Teflon-lined stainless autoclave. The molar ratio of NH_4VO_3 to EDTA was 6 and the pH value of the solution was about 2.5. Then the hydrothermal reaction proceeded at 180 °C for 12 h. After the autoclave was cooled to room temperature naturally, the alumina substrate coated with VO_2 nanobelts was taken out and rinsed, and then dried at 80 °C for 6 h in a vacuum. To further prepare the V_2O_5 nanobelts, the above VO_2 nanobelts were heated at 350 °C in air for 1 h, and then cooled naturally. The samples were characterized with a field emission scanning electron microscope (FESEM, Hitachi S4800), x-ray diffraction (XRD, RIGAKU D/MAX 2500V/PC, Cu Kα radiation), and field emission transmission electron microscopy (FETEM, TECNAI G^{2}F-20).

Gas-sensing properties of V_2O_5 nanobelt networks were investigated in a home-built static gas-sensing characterization system as shown in our previous work.[18] The sensor was placed on the heating plate and a predetermined amount of ethanol gas was introduced into the chamber directly to reach a desired concentration. The resistance change of the sensor was continuously monitored by a programmable digital multimeter in the whole measurement process. The sampling interval was set to be 1 s and the test temperature was changed from 100 °C to 300 °C by adjusting the temperature controller of the heating plate. During the measurement, the ambient relative humidity was about 35%–40%.

3. Results and discussion

3.1. Structure characterization

Figure 1(a) shows the XRD patterns of the as-synthesized VO_2 nanobelts. All the peaks can be well indexed to the monoclinic phase of VO_2 (JCPDS No. 65-7960). The XRD pattern in Fig. 1(b) shows a pure orthorhombic V_2O_5 (JCPDS No. 41-1426), indicating that the annealing at 350 °C results in a complete transformation of monoclinic VO_2 to orthorhombic V_2O_5. It is thought that the phase transformation under the gentle annealing is related to the unique ultrathin feature of VO_2 nanobelts. Strong and sharp XRD peaks in Figs. 1(a) and 1(b) indicate the good crystallinities of the samples.

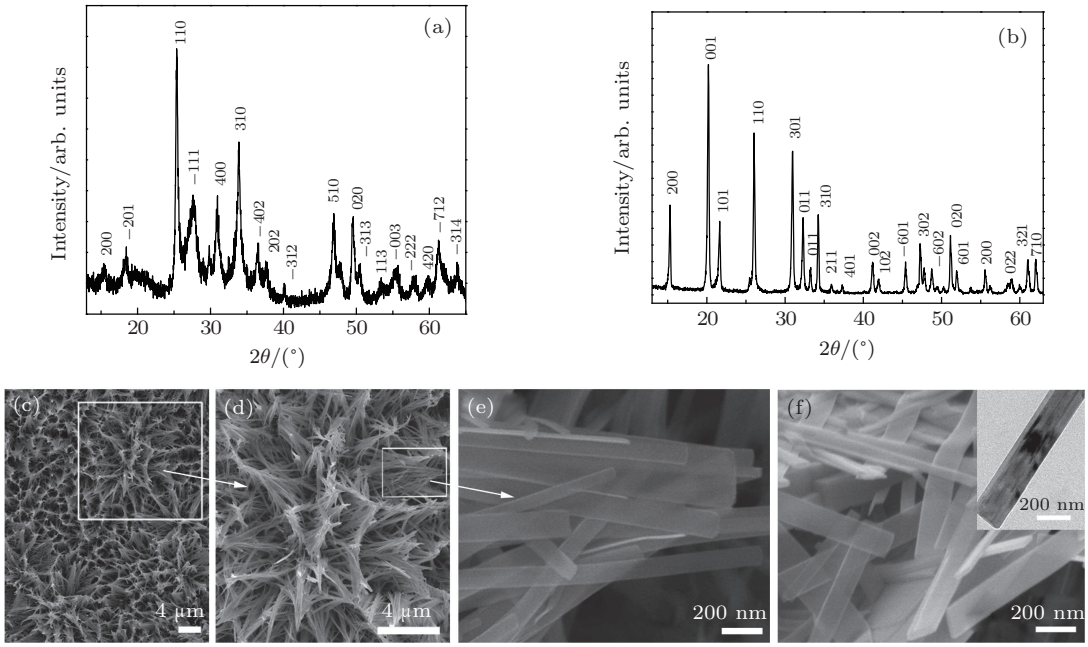


Fig. 1. XRD patterns and SEM images of (a), (c)–(e) VO_2 nanobelts, (b) and (f) V_2O_5 nanobelts. The inset in panel (f) shows the TEM image of a single bundle of stacked V_2O_5 nanobelts.

Figures 1(c)–1(e) show the typical scanning electron microscope (SEM) images of the VO_2 nanobelts. The low-magnification images in Figs. 1(c) and 1(d) reveal a homogeneous phase of well-defined nanobelts with lengths on the order of several micrometers. The nanobelts grow upward and display a rough alignment morphology. The enlarged SEM image in Fig. 1(e) clearly shows that the VO_2 nanobelts have thickness values ranging from 10 nm to 20 nm and widths

in a range of 50 nm–150 nm. Notably, the as-synthesized VO_2 nanobelts are ultrathin, as evidenced by the nearly semi-transparent appearance. This kind of ultrathin-structured 1D nanobelt is very favorable for applications in nanoelectronic and nanophotonic devices due to the extremely high surface-to-volume ratio. Furthermore, the ultrathin feature ensures the following successful transformation of a VO_2 nanobelt into a V_2O_5 nanobelt with a nearly unchanged morphology under a mild annealing at 350 °C. The high magnification SEM image in Fig. 1(f) shows that the V_2O_5 nanobelts still keep semitransparent. Some thicker nanobelts are distinguished to be composed of several ultrathin nanobelts with face-to-face stacking. The inset in Fig. 1(f) gives the TEM image of a single bundle of stacked V_2O_5 nanobelts. Its legible microstructure indicates that the mild annealing at 350 °C avoids the lattice coalescence of adjacent nanobelts and maintains the original ultrathin feature of the nanobelts. The presented ultrathin V_2O_5 nanobelt is expected to be a promising candidate for a high sensitive gas sensor due to its perfect single crystal structure and limited thickness comparable to the Debye length.

Figures 2(a), 2(b), 2(c), and 2(d) respectively give the TEM images of VO_2 and V_2O_5 nanobelts. The nanobelts of VO_2 and V_2O_5 show themselves to have nearly rectangle ends, and the ultrathin structure could be further confirmed from Figs. 2(a) and 2(c). The selected area electron diffraction (SAED) pattern in the inset of Fig. 2(b), taken from a single nanobelt marked in Fig. 2(a), verifies that the VO_2 nanobelts are comprised of monoclinic crystals of VO_2 with a preferential growth along the (110) direction. Similarly, the SAED pattern in the inset of Fig. 2(c) demonstrates that the V_2O_5 nanobelts are orthorhombic and grow preferentially along the *c* direction. The sharp diffraction spots and the highly periodic lattice structures shown in Figs. 2(b) and 2(d) reveal the perfect single crystal natures of VO_2 and V_2O_5 nanobelts. The *d*-spacing of 0.35 nm in Fig. 2(b) and 0.43 nm in Fig. 2(d) are respectively consistent with those of the (110) plane of monoclinic VO_2 and the (001) plane of orthorhombic V_2O_5. The above results are quite consistent with those from the SEM and XRD characterizations.

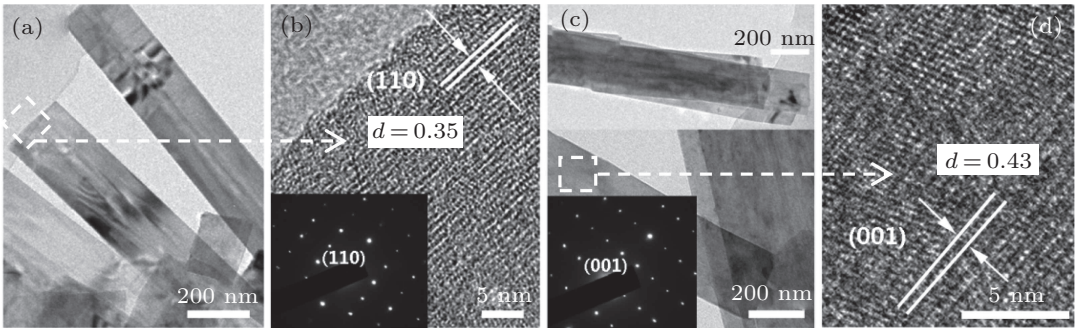


Fig. 2. TEM images of (a) and (b) VO_2 nanobelts, (c) and (d) V_2O_5 nanobelts. The insets in panels (b) and (c) show the corresponding SAED patterns of the VO_2 nanobelt and the V_2O_5 nanobelt, respectively.

Owing to the chelating and capping effect, in this work, EDTA is chosen to serve as a medium to facilitate the growth of 1D VO_2 nanobelts. The concentration of EDTA is found to be crucial in controlling the VO_2 morphology. SEM images in Figs. 3(a) and 3(b) show the samples obtained at molar ratios of NH_4VO_3 to EDTA of 6 and 2, respectively. Clearly, the morphologies of the samples are highly corrective with the initial concentration of EDTA. Under low EDTA concentration (NH_4VO_3/EDTA = 6), 1D ultrathin nanobelts with an average thickness in a range of 10 nm–20 nm and width in a range of 50 nm–150 nm are formed as described above. Increasing the initial concentration of EDTA, preferential growth tendency for VO_2 crystal is weakened evidently. A much higher concentration of EDTA (NH_4VO_3/EDTA = 2) induces the formation of thick nanoplates as indicated in Fig. 3(b). The enlarged rectangular cross sections show the thickness and width of the nanoplates are in ranges of 80 nm–120 nm and 0.8 μm–1.5 μm, respectively.

The possible growth process of the 1D nanobelts is proposed in Fig. 3. As shown in the SEM images, both nanobelts and nanoplates exhibit roughly aligned morphologies. While based on an unannealed induction layer, only a disordered nanobelts network parallel to the substrate is obtained (not shown here). Therefore, the annealed induction layer plays a key role in directing aligned growth of VO_2 nanostructures. The rough surface induced from the annealed induction layer is assumed to provide the initial nucleation sites to inspire the upward crystal growth, owing to the local enhanced adsorption of reactant ions on it.[19,20] Subsequent growth of vanadium oxide is effectively mediated by EDTA in hydrothermal solution. EDTA is known to possess a strong chelating capability with metal ions, and meanwhile serve as a capping agent to control the anisotropic growth of crystal via the selective interaction with specific crystallographic planes.[14,21] Under a

low EDTA concentration, the EDTA only preferentially cap on some special planes and suppress the crystal growth in this direction, forming ultrathin 1D nanobelts (Fig. 3(a)). When the EDTA concentration is much higher, other facets are expected to be capped (Fig. 3(b)). Consequently, the growth rates of different facets tend to be balanced and the energy difference among crystal faces decreases. That is, growth tendencies along various directions tend to be equalized. It is evident from Fig. 3 that excess EDTA facilitates the formation of VO_2 nanoplates with larger thickness.

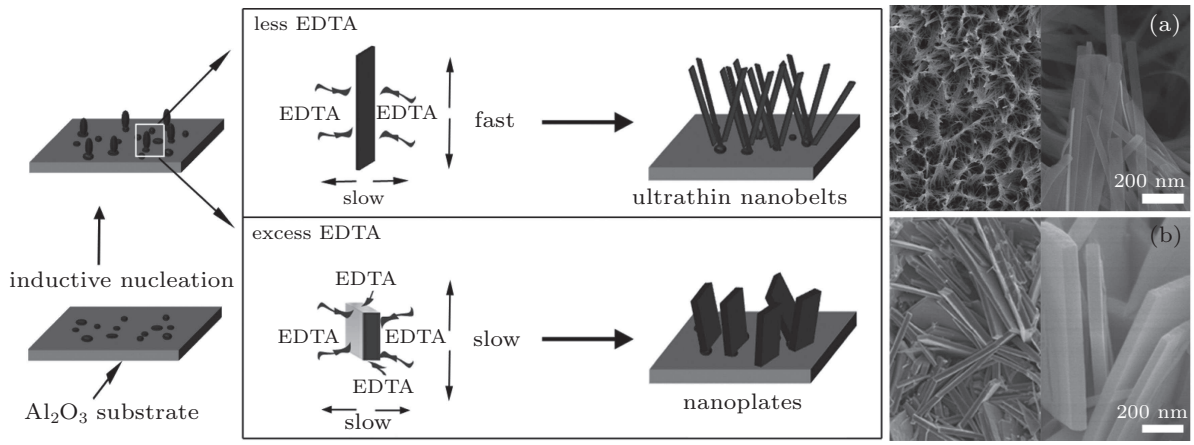


Fig. 3. (color online) Schematic illustration of the *in-situ* formation mechanism of VO_2 samples: (a) ultrathin nanobelts, NH_4VO_3/EDTA = 6:1, and (b) nanoplates, NH_4VO_3/EDTA = 2:1.

3.2. Gas-response properties

Gas-sensing properties of the V_2O_5 nanobelt networks are based on the resistance changes before and after the test gas is injected. To explore the optimum operating temperature, the sensor response of V_2O_5 nanobelt networks to 250-ppm ethanol gas is first measured at different operating temperatures. Figure 4 shows the relationship between the sensor response and operating temperature for the as-synthesized V_2O_5 nanobelt networks toward 250-ppm ethanol gas from 100 °C to 300 °C. Here, the sensor response is defined as $S = R_a/R_g$, where R_a and R_g are the resistances of the as-prepared gas sensor in the ambient air and in the ethanol gas, respectively. As observed in the figure, the V_2O_5 nanobelt network sensor shows an optimal operating temperature of 250 °C, at which the maximum response value of 9.8 is achieved. Such an operating temperature is lower than those of V_2O_5 thin films and most metal oxides.[22,23]

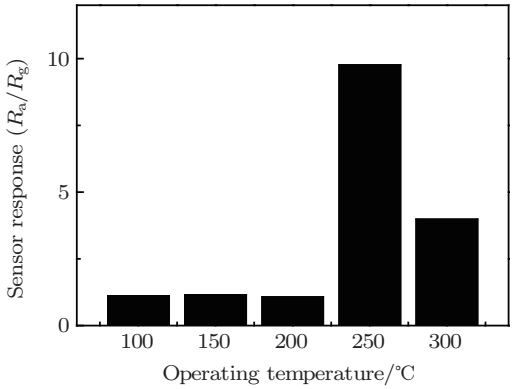


Fig. 4. Relationship between the sensor response and operating temperature for V_2O_5 nanobelt networks toward 250-ppm ethanol gas.

Figure 5 shows the dynamic responses of the gas sensor when exposed to ethanol gas at the optimal working temperature of 250 °C. As shown in the figure, the measured resistances of the gas sensor decrease upon exposure to ethanol gas, which shows the typical feature of an n-type semiconductor. It is also noted that the as-prepared V_2O_5 nanobelt network sensor exhibits a very good response–recovery characteristic, especially a very rapid response characteristic. The response time, defined as the time required for the resistance of the sensor to reach 90% of the equilibrium value after the test gas has been injected, varies in a range of 10 s–25 s. After the removing of ethanol gas, the sensor could return to its initial resistance value. We can see that even after five test cycles using different concentrations of ethanol, the resistance of the gas sensor can almost recover to its initial value, indicating the excellent reversibility and stability of the sensor based on V_2O_5 nanobelt networks. The perfect stability and reversibility are attributed greatly to the good interface performance between the electrodes and the nanobelts including good adhesion and electrical contact resulting from the directly bottom-up growth of V_2O_5 nanobelts on the substrate.[24]

Another point that is important to note in Fig. 5 is that the sensor described here is responsive to extremely dilute ethanol gas (3 ppm) at 250 °C, which is far below the limit imposed on the breath analyzer (200 ppm).[7] It indicates that the sensor based on the presented ultrathin V_2O_5 nanobelts networks is indeed capable of detecting dilute ethanol of several ppm levels. Figure 6 displays the gas responses of V_2O_5 nanobelt networks to different concentrations of ethanol (3 ppm–500 ppm), showing that the sensor response increases rapidly with the rise of the ethanol concentration, especially when the concentration is below 100 ppm, which further suggests that the sen-

sor could meet the application demand for monitoring the dilute ethanol gas.

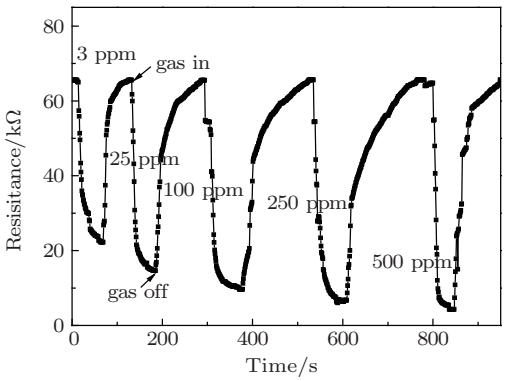


Fig. 5. Dynamic responses of the gas sensor based on V_2O_5 nanobelt networks to varying ethanol concentrations at the optimal operating temperature of 250 °C.

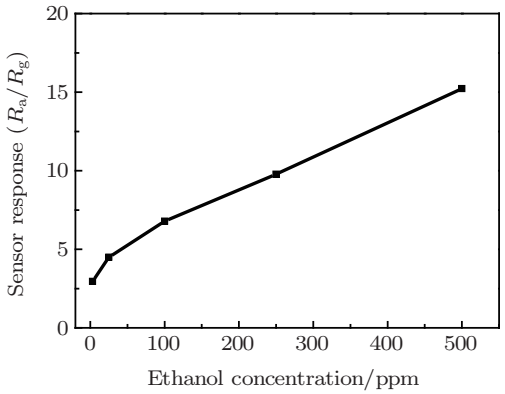


Fig. 6. Relationship between sensor response and ethanol concentration for the V_2O_5 nanobelt network sensor at an optimal working temperature of 250 °C.

It is thought that the efficient utilizations of the surface area and surface accessibility are crucial to maintain the high sensitivity and fast response characteristic of a gas sensor.[25] Thus, the excellent response capability to dilute ethanol gas and fast recovery characteristic could be understood considering the unique structural features of the rough aligned, ultrathin V_2O_5 nanobelt networks. Ultrathin nanobelt networks can supply a large number of surface active sites facilitating the adsorption of gas molecules due to their high effective surface area. This is favorable for achieving a high gas-sensitivity. Meanwhile, the loose structure of the rough aligned nanobelts, which are assembled by the directly bottom-up growth on the substrate, allows the gas to diffuse agilely in the sensing networks. That is, the gas molecules can be effectively adsorbed on and swept away from the surface of V_2O_5.[21] As a result, fast response and recovery are achieved.

4. Conclusions

A novel two-step process, i.e., *in-situ* inductive nucleation followed by EDTA-mediated hydrothermal growth, is developed to prepare ultrathin and aligned VO_2 nanobelts on a substrate. The performed inductive layer is crucial for aligned growth of nanobelts; meanwhile EDTA serves as a capping agent to facilitate the preferential growth of 1D VO_2 nanobelts. With mild annealing at 350 °C in air, the as-synthesized ultrathin VO_2 nanobelts could transform into ultrathin V_2O_5 nanobelts. The possible formation mechanism of VO_2 nanobelts is proposed by involving the crucial guide role of EDTA in crystal growth. Owing to the good interface performance and gas adsorption–desorption properties, the as-prepared V_2O_5 nanobelt network exhibits excellent reversibility and stability, high response value, and fast response–recovery characteristic to ethanol gas at its optimal operating temperature of 250 °C. Thus, the presented ultrathin and rough aligned V_2O_5 nanobelt networks are considered as a promising sensing material in developing an ethanol sensor with low power consumption, excellent sensitivity, and good gas stability.

References

[1] Schoch Rebo B, Han Jongyoon and Renaud Philippe 2008 *Rev. Mod. Phys.* **80** 839
[2] Cui Y, Charles M and Lieber 2001 *Science* **291** 851
[3] Pu C Y, Zhou D W, Bao D X, Lu C, Jin X L, Su T C and Zhang F W 2014 *Chin. Phys. B* **23** 026201
[4] Tang X Y, Gao H, Wu L L, Wen J, Pan S M, Liu X and Zhang X T 2015 *Chin. Phys. B* **24** 394
[5] Nagaraju G, Chithaiahb P, Mahadevaiah N and Ashokac S 2012 *Cryst. Res. Technol.* **47** 868
[6] Li B X, Xu Y, Rong G X, Jing M and Xie Y 2006 *Nanotechnology* **17** 2560
[7] Liu J F, Wang X, Peng Q and Li Y D 2006 *Sens. Actuators B* **115** 481
[8] Zhang Y F, Zhang X Z, Huang Y, Huang C, Niu F, Meng C G and Tan X Y 2014 *Solid State Commun.* **180** 24
[9] Qin M L, Liang Q, Pan A Q, Liang S Q, Zhang Q, Tang Y and Tan X P 2014 *J. Power Sources* **268** 700
[10] Mjejri I, Etteyeb N and Sediri F 2014 *Mater. Res. Bull.* **60** 97
[11] Zeng M, Yin H H and Yu K 2012 *Chem. Eng. J.* **188** 64
[12] Shi S F, Cao M H, He X Y and Xie H M 2007 *Cryst. Growth Des.* **7** 1893
[13] Thirumalai J, Chandramohan R and Vijayan T A 2011 *Mater. Chem. Phys.* **127** 259
[14] Luo F, Jia C J, Song W, You L P and Yan C H 2005 *Cryst. Growth Des.* **5** 137
[15] Wang X H, Sang Y H, Wang D Z, Ji S Z and Liu H 2015 *J. Alloys Compd.* **639** 571
[16] Kang Z H, Wang E B, Mao B D, Su Z G, Gao L, Lian S Y and Xu L 2005 *J. Am. Chem. Soc.* **127** 6534
[17] Li G C, Pang S P, Jiang L, Guo Z Y and Zhang Z K 2006 *J. Phys. Chem. B* **110** 9383
[18] Qin Y X, Fan G T, Liu K X and Hu M 2014 *Sens. Actuators B* **190** 141
[19] Yue J, Jiang X C and Yu A 2012 *J. Phys. Chem. C* **116** 8145
[20] Kaneti Y V, Zakaria Q M D, Zhang Z, Chen C and Liu M 2014 *J. Mater. Chem. A* **2** 13283
[21] Deng H, Liu C, Yang S, Xiao S, Zhou Z and Wang Q 2008 *Cryst. Growth Des.* **8** 4432
[22] Abbasi M, Rozati S M, Irani R and Beke S 2015 *Mater. Sci. Semicond. Process.* **29** 132
[23] Wang C H, Yin L, Zhang L, Xiang D and Gao R 2010 *Sensors* **10** 2088
[24] Choi Y J, Hwang I S, Park J G, Choi K J, Park J H and Lee J H 2008 *Nanotechnology* **19** 095508
[25] Lee J H 2009 *Sens. Actuators B: Chemical* **140** 319